World Journal of Surgical Oncology

RESEARCH

Open Access

DCC-2036 inhibits osteosarcoma via targeting HCK and the PI3K/AKT-mTORC1 axis to promote autophagy

Jun He[1,2†], Liyang Yin[3†], Qiong Yuan[3], Xiaotao Su[2], Yingying Shen[3*] and Zhongliang Deng[1*]

Abstract

Background Osteosarcoma is a common bone tumor in adolescents and children, characterized by rapid progression, high malignancy, poor prognosis, and a tendency for pulmonary metastasis. Despite extensive research efforts, the specific driver gene associated with osteosarcoma remains unidentified, underscoring the urgent need for novel therapeutic targets and targeted treatment options.

Methods In vitro studies were conducted to assess the effects of DCC-2036 on the proliferation, migration, and invasion of osteosarcoma (OS) cell lines, employing cloning and Transwell experiments. Network pharmacological analysis, complemented by in vitro experimental validation, indicated the critical target responsible for the inhibitory effects of DCC-2036. RNA sequencing analysis demonstrated that DCC-2036 could induce autophagy in OS cells, with relative protein levels assessed using Western blotting following treatment with the autophagy inhibitor 3-MA and the mTOR agonist MHY1485. In vivo studies further confirmed the role of DCC-2036 in cell proliferation through subcutaneous tumorigenesis.

Results In this study, we demonstrated that the small molecule tyrosine kinase inhibitor DCC-2036 effectively inhibited osteosarcoma (OS) cells in both cellular and animal models. We found that DCC-2036 significantly suppressed the proliferation of osteosarcoma cells and induced apoptosis; additionally, it notably inhibited cell migration, invasion, and epithelial-to-mesenchymal transition (EMT). HCK was identified as the key target mediating the effects of DCC-2036 on osteosarcoma. Mechanistically, DCC-2036 was shown to inhibit the expression of phosphorylated AKT (p-AKT), phosphorylated S6 kinase (p-S6K), and phosphorylated 4E-binding protein 1 (p-4EBP1) within the downstream PI3K/AKT/mTORC1 signaling pathway. Furthermore, in vivo experiments utilizing subcutaneous tumor xenografts in mice demonstrated that DCC-2036 effectively inhibited the growth of xenografted 143B cells in BALB/C-nude mice.

†Jun He and Liyang Yin contributed equally to this work.

*Correspondence:
Yingying Shen
shenyingying1113@usc.edu.cn
Zhongliang Deng
dengzhongliang0107@126.com

Full list of author information is available at the end of the article

Conclusions Collectively, these findings indicate that DCC-2036 promotes autophagy in osteosarcoma (OS) cells by targeting the HCK/AKT/mTORC1 axis and exerts anti-tumor effects without significant toxicity. Consequently, DCC-2036 emerges as a promising therapeutic agent for the treatment of HCK-overexpressing osteosarcoma.

Keywords DCC-2036, HCK, Osteosarcomas (OS), Autophagy

Introduction

Osteosarcomas (OS) account for approximately 20-40% of all bone tumors, predominantly affecting children and adolescents [1, 2]. This type of tumor is characterized by rapid progression, a high level of malignancy, poor prognosis, and the occurrence of lung metastases [3, 4]. Surgical treatment and chemotherapy remain the standard approaches for managing osteosarcoma [5, 6]. Currently, methotrexate, cisplatin, doxorubicin, and ifosfamide are the mainstays of OS chemotherapy. However, the clinical application of chemotherapy is significantly limited due to high resistance and severe toxic side effects, including ototoxicity, nephrotoxicity, cardiotoxicity, and neurotoxicity [7, 8]. In recent years, molecular targeted therapy has shown promising results in enhancing prognosis and tumor management [9, 10]. Nonetheless, the driver genes (targets) of osteosarcoma remain unclear, making the identification of new targets and targeted therapeutic agents an urgent challenge in osteosarcoma research.

Protein tyrosine kinases play a crucial role in cellular signal transduction pathways, regulating various physicochemical processes such as cell growth, differentiation, and apoptosis [11]. The excessive amplification or mutation of the gene encoding tyrosine kinase can lead to sustained increases in tyrosine kinase activity, consequently inducing tumorigenesis [12, 13]. Therefore, the development of drugs targeting tyrosine kinases has increasingly become a focal point in anti-tumor drug research [14, 15]. Notably, several prospective phase II trials of tyrosine kinase inhibitors (TKIs) have been conducted for osteosarcoma, including regorafenib, cabozantinib, sorafenib (with or without everolimus), apatinib, and lenvatinib, which primarily target VEGFR and its downstream signaling pathways [16, 17].

DCC-2036 (Rebastinib) is a third-generation tyrosine kinase inhibitor specifically designed to target ABL1 in chronic myeloid leukemia (CML) [18]. Our previous studies demonstrated that DCC-2036 exerts anti-tumor activity against triple-negative breast cancer (TNBC) by targeting AXL/MET, thereby regulating the downstream PI3K/Akt-NFκB pathway [19]. Additionally, it inhibits TNBC stem cells by disrupting the AXL-KLF5 positive-feedback loop [20]. As a multi-target inhibitor, DCC-2036 can also inhibit the activity of various tyrosine kinases that are highly expressed in osteosarcoma, including SRC, PDGFRα, and VEGFR2/KDR [18]. Consequently, we hypothesize that DCC-2036 may also exert a significant inhibitory effect on osteosarcoma. In this study, we evaluated the efficacy of DCC-2036 against osteosarcoma both in vitro and in vivo, elucidating the critical targets and molecular mechanisms involved.

Methods

Chemicals and antibodies

DCC-2036 was purchased from Selleck (Houston, TX), while MHY1485 and 3-MA were obtained from MCE (Shanghai, China). These compounds were dissolved in DMSO and stored at -20 °C. The Western blot antibodies used in this study included phospho-AKT (S473) #4060, Vimentin #5741, and ZEB1 #3396, all sourced from Cell Signaling Technology (Beverley, MA). Additionally, GAPDH #60004-1-Ig, β-actin #66009-1-Ig, 4EBP1 #60246-1-Ig, Snail #13099-1-AP, P70(S6K) #14485-1-AP, P62 #18420-1-AP, AKT #10176-2-AP, VEGFR2/KDR #26415-1-AP, and E-Cadherin #20874-1-AP were acquired from Proteintech (Wuhan, China). Furthermore, HCK #AF7711, phospho-HCK (Tyr522) #AF7211, phospho-4EBP1 (Thr37/Thr46) #AF3830, phospho-p70 S6K (Thr389/Thr412) #AF3228, and phospho-VEGFR2 (Tyr1175) #AF4426 were purchased from Affinity (Changzhou, China). Lastly, LC3B #A19665 was obtained from ABclonal (Wuhan, China).

Cell culture

Human osteosarcoma cell lines MG-63 and 143B were obtained from ATCC and cultured in DMEM (Gibco, Waltham, MA), supplemented with 10% fetal bovine serum (HAKATA, Shanghai, China) and 1% penicillin/streptomycin. The cultures were maintained at 37 °C in a 5% CO2 atmosphere.

Cell treatment

Cells were plated in six-well plates and incubated overnight at 37 °C in a 5% CO2 atmosphere. Once they reached 70–80% confluence, the cells were treated with varying concentrations of DCC-2036 (0 μM, 2.5 μM, 5 μM, 10 μM)for 48 h, 3mM 3-MA for 3 h, and 10 μM MHY1485 for 6 h.

Cell viability assay

Cell viability was assessed using the CCK-8 assay (Abbkine, Wuhan, China). Cells in the logarithmic growth phase were trypsinized and resuspended in a cell suspension. Subsequently, 3,000 cells were seeded into each well of a 96-well plate and incubated overnight at 37 °C in a 5% CO2 environment until they adhered to the surface.

The peripheral wells were filled with sterile PBS. Drug treatment involved dilutions of concentrations ranging from 0 to 20 μM, with three replicates for each concentration, and lasted for 72 h. Following treatment, 10 μL of CCK-8 solution was added and incubated for 2 h in the incubator. The absorbance was measured with a 96-well plate reader at a wavelength of 450 nm. The 50% inhibition of cell growth (IC50) value was calculated using GraphPad Prism software.

Colony formation assay

The MG63 and 143B cells were seeded in 6-well plates and treated with varying concentrations of DCC-2036 for 48 h. Following this, the cells were treated with 30 μM of 3-MA for 3 h, and subsequently exposed to 10 μM of MHY1485 for 6 h. After treatment, the cells were harvested, washed, and cultured in drug-free DMEM medium. After a 7-day incubation period, the cells were washed again, fixed, and stained. Finally, the number of colonies was quantified using an inverted microscope, with colonies containing 50 or more cells being counted.

Flow cytometry

Control group cells and those treated with DCC-2036 or DCC-2036 combined with 3-MA underwent digestion, collection, and washing with PBS. Annexin V-FITC and PI were subsequently introduced to interact with the cells at room temperature in the absence of light, followed by the detection of apoptotic cells using flow cytometry.

Transwell assay

The transwell cell culture chambers were prepared with Matrigel for invasion assays and without Matrigel for migration assays. Osteosarcoma cell lines (MG63 and 143B) were treated with 2.5 and 5 μM DCC-2036 for 48 h and subsequently harvested in serum-free medium. A suspension of 300 μL of cells and 20 μL of Matrigel was introduced into each upper chamber for invasion assays (with no Matrigel for migration assays), while 500 μL of culture medium containing 10% FBS was added to the lower chamber. Following a 48-hour incubation period at room temperature, the transwell chambers were removed, and cells on the upper membrane were gently wiped away with a cotton swab after washing. The infiltrated cells on the lower surface were treated with 95% alcohol for 10 min, stained with a 0.5% crystal violet solution for 5 min, and counted using an inverted microscope (five fields per chamber at 100× magnification).

Western blotting

Radioimmunoprecipitation (RIPA) buffer was utilized to prepare the whole cell lysate from the collected cells. The protein concentration was quantified using the BCA method (Cwbio, Wuhan, China). The protein lysate was then separated by SDS-PAGE and transferred to a PVDF membrane. The PVDF membrane was subsequently incubated with the corresponding antibody. The blots were detected using the ECL Detection System (Abbikine, Wuhan, China).

Immunofluorescence

Sterilized cell sheets were initially placed in a petri dish, followed by the digestion of cells in the logarithmic growth phase using trypsin to prepare a cell suspension. Subsequently, 1 × 10^6 cells per well were inoculated into 6-well plates and cultured in a CO2 incubator (5%) at 37 °C for 24 h. After this incubation period, the cells were treated with 2.5 μM DCC-2036 for 48 h, fixed with 4% paraformaldehyde for 20 min, permeabilized with 0.5% Triton X-100, and washed three times with PBS. The cells were then blocked with 3% BSA for 30 min, incubated with the primary antibody overnight, and stained with the secondary antibody for 1 h. The incubation was concluded by washing three times with PBS, adding an antifluorescence quenching agent, and subsequently observing the slides under a fluorescence microscope.

Tumor xenograft models

0.2 ml of 143B cells suspension with the concentration of 1×10^7 cells/ml were transplanted subcutaneously into the right side of backs of female BALB/c nude mice aged 6 weeks. Upon reaching a subcutaneous tumor volume of 50–100 mm^3, the mice were randomly assigned to either a control group or a drug group. Daily measurements of weight and tumor volume were recorded. The drug group received a specified daily dosage of DCC-2036, while the control group received an equivalent volume of drug solvent. The experiment concluded when the control group reached a tumor volume of 1200 mm^3, resulting in the euthanization of nude mice across all groups. The subcutaneous tumors were excised, documented, weighed, and a portion of the tissue was preserved for immunohistochemical analysis of protein expression. Another portion was utilized for Western Blot analysis of key proteins. All animal experiments were approved by the Medical Ethics Committee of Nanhua Hospital, University of South China (2023-KY-120).

Statistical analysis

GraphPad Prism software 8 was used for statistical analysis. Comparisons between two groups involved Student's t-test. P value was defined as $^{*}p < 0.05$, $^{**}p < 0.01$, $^{***}p < 0.001$, $^{****}p < 0.0001$.

Results

DCC-2036 significantly inhibited the proliferation and induced apoptosis in osteosarcoma cells

This study aimed to investigate the effects of DCC-2036 on the proliferation of osteosarcoma cells. The results revealed that the IC50 values for inhibiting the growth of the osteosarcoma cell lines 143B and MG63 were 2.59 μM and 1.431 μM, respectively (Fig. 1a). The plate cloning assay demonstrated a reduction in colony formation with increasing concentrations of DCC-2036, indicating a significant inhibition of osteosarcoma cell proliferation (Fig. 1b). Furthermore, flow cytometry analysis indicated a dose-dependent increase in apoptosis induced by DCC-2036 (Fig. 1c).

DCC-2036 significantly inhibited osteosarcoma cell migration, invasion and EMT

DCC-2036 exhibited significant inhibitory effects on the migration and invasion of 143B and MG63 cells, as demonstrated by Transwell assays. Furthermore, a dose-dependent relationship was observed, indicating that higher concentrations of DCC-2036 led to increased inhibition of cell migration and invasion (Fig. 2a-b). Subsequent Western blot analysis revealed alterations in epithelial-mesenchymal transition (EMT) markers in 143B and MG63 cells treated with DCC-2036. Specifically, an upregulation of E-cadherin expression and a downregulation of ZEB1, Vimentin, and Snail expression were observed, suggesting that DCC-2036 effectively inhibits the progression of EMT (Fig. 2c).

The potential target of DCC-2036 in the inhibition of osteosarcoma was analyzed using network pharmacology revealing HCK as the key target

The Swiss database identified 100 effective targets of DCC-2036, with only the top 10 targets displayed in Fig. 3a. Differential enrichment analysis was performed on 3 cases of osteoblastoma (OB) and 15 cases of osteosarcoma (OS) from the GSE9460 dataset, leading to the identification of 3,310 differentially expressed genes. Among these genes, 1,576 were found to be highly expressed, while 1,734 were under-expressed (Fig. 3b). The heat map illustrated the expression of the top 20 Differentially Expressed Genes (DEGs) in the samples (Fig. 3c), and Principal Component Analysis (PCA) along with Uniform Manifold Approximation and Projection (UMAP) demonstrated significant differences in distribution between the two groups of samples (Figs. 3d-e). The results from the Venn Diagram indicated that 17 'potential DEGs' were identified, including HCK, CTSK, TRPV1, FLT1, PDE4B, IDH1, PTK2B, ACACA, MERTK, MAPK9, MAPK14, CTSS, CDC42BPG, TNKS, KDR, PDE11A, and CSF1R (Fig. 3f). These findings suggest that these genes may serve as potential targets for DCC-2036 in the inhibition of osteosarcoma.

The interaction of 17 potential target genes was analyzed using the STRING database, revealing that 10 of these genes exhibited interactions (Fig. 4a). A topological analysis was conducted utilizing the Cytohubba plug-in, identifying the top five genes with the strongest interaction capabilities—referred to as key genes: HCK, MAPK14, PTK2B, KDR, and CSF1R (Figs. 4b-c). Notably, HCK, MAPK14, KDR, and CSF1R are highly expressed in osteosarcoma (OS), whereas PTK2B is expressed at low levels in OS (Fig. 4d). This suggests that DCC-2036 may play a role in osteosarcoma intervention by down-regulating HCK, MAPK14, KDR, and CSF1R, or by up-regulating PTK2B.

Furthermore, a combination of multiple databases was employed, and AutodockTools software was used to perform docking simulations of DCC-2036 with HCK, MAPK14, PTK2B, KDR, and CSF1R to elucidate its binding affinity. The results indicated that all five genes were capable of successfully docking with DCC-2036 under physiological conditions (binding energy < 0 kcal/mol) (Fig. 4e). The visualization of the docking results for DCC-2036 with HCK, MAPK14, PTK2B, KDR, and CSF1R was conducted using PyMOL software (Figs. 4f-j). The findings demonstrated that DCC-2036 forms hydrogen bonds with the 21st amino acid (Valine, VAL) of CSF1R, the 518th amino acid (Threonine, THR) of HCK, and the 18th amino acid (Phenylalanine, PHE) of KDR. Additionally, it binds to amino acids 88, 89, 91, and 94 of MAPK14 (Aspartate, ASP; Valine, VAL; Threonine, THR; Arginine, ARG) through hydrogen bonding, as well as to amino acids 50, 54, and 206 of PTK2B (Phenylalanine, PHE; Lysine, LYS; Lysine, LYS) through hydrogen bonding interactions.

In vitro kinase experiments of DCC-2036 have demonstrated that only HCK (40 nM) and KDR (4 nM) exhibit an IC50 < 100 nM [1]. Western blot analysis indicated a significant decrease in both p-HCK and HCK levels following treatment with DCC-2036 in 143B cells, while p-KDR and KDR levels exhibited minimal changes (Fig. 4k). These findings suggest that HCK may represent a critical target of DCC-2036 for the inhibition of osteosarcoma.

DCC-2036 effectively inhibited the activity of osteosarcoma cells by inducing autophagy through the suppression of the PI3K-AKT-mTORC1 signaling pathway

To elucidate the specific molecular mechanisms by which DCC-2036 regulates osteosarcoma proliferation, apoptosis, invasion, and metastasis, we performed transcriptome sequencing on 143B cells treated with DCC-2036. The analysis identified a total of 6,287 up-regulated genes and 435 down-regulated genes exhibiting

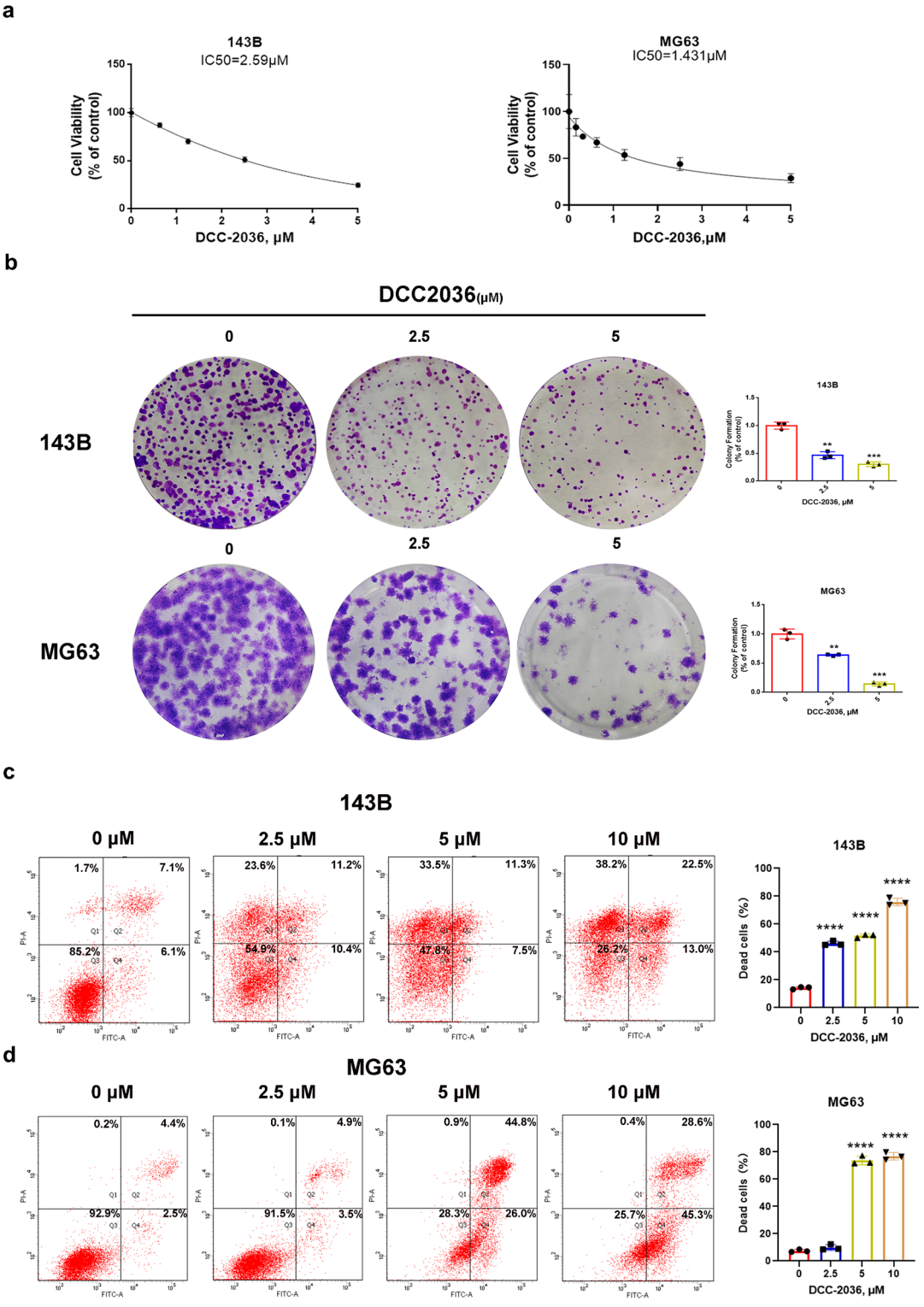

Fig. 1 DCC-2036 inhibits proliferation and induces apoptosis of osteosarcoma cells **a**. The growth of osteosarcoma cells was inhibited by DCC-2036. 143B and MG63 cells were exposed to varying concentrations of DCC-2036 for 72 h, after which a CCK8 assay was performed. Data were collected from three independent experiments and are presented as mean ± standard deviation (SD). **b.** The clonal formation of osteosarcoma cells was suppressed by DCC-2036. Osteosarcoma cells were treated with DCC-2036 at concentrations of 0 μM (control group), 2.5 μM, and 5 μM for 48 h, and the number of cell colonies was determined through three repetitions, reported as mean ± standard deviation (SD). The image provides a schematic representation of three distinct experiments involving the formation of clones. **c.** Osteosarcoma cells were subjected to varying concentrations of DCC-2036 for 48 h, followed by Annexin V-FITC/PI double staining. The left panel illustrates a representative graph from the three independent experiments, while the right panel displays the corresponding statistical analysis, with significance levels denoted as $^{**}p < 0.01$, $^{***}p < 0.001$, and $^{****}p < 0.0001$

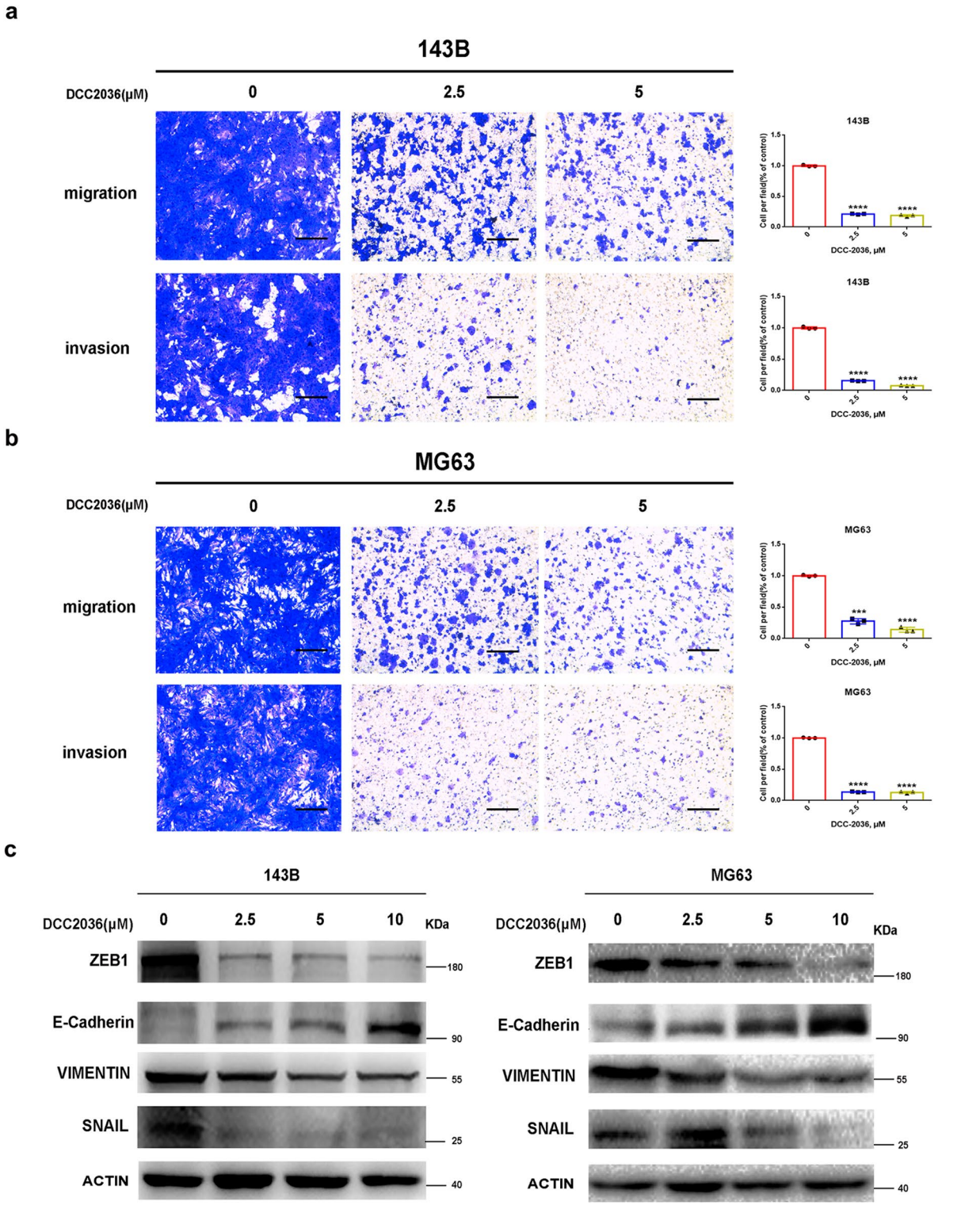

Fig. 2 DCC-2036 inhibits osteosarcoma cell migration, invasion and epithelial-mesenchymal transition (EMT) **a-b.** The invasion and migration of 143B and MG63 cells treated with DCC-2036 at varying concentrations (0 μM, 2.5 μM, 5 μM) were assessed using Transwell assays. Representative plots from three independent experiments are displayed on the left, while statistical analyses of cell numbers are presented on the right. Statistical significance was determined using a t-test, with significance levels denoted as $*p < 0.05$, $***p < 0.001$, and $****p < 0.0001$. Images were captured at a magnification of 400× with a scale bar of 100 μm. **c.** Changes in EMT marker expression in 143B and MG63 cells treated with DCC-2036 at different concentrations (0 μM, 2.5 μM, 5 μM, 10 μM) were evaluated using Western blot assays

a

SwissTargetPrediction						
Target	**Common name**	**Uniprot ID**	**ChEMBL ID**	**Target Class**	**Probability***	**Known actives (3D/2D)**
Tyrosine-protein kinase YES	YES1	P07947	CHEMBL2073	Kinase	0.341815253	11 / 2
MAP kinase p38 alpha	MAPK14	Q16539	CHEMBL260	Kinase	0.216999568	419 / 290
Serine/threonine-protein kinase B-raf	BRAF	P15056	CHEMBL5145	Kinase	0.154562075	136 / 15
Tyrosine-protein kinase ABL	ABL1	P00519	CHEMBL1862	Kinase	0.136785586	96 / 23
Focal adhesion kinase 1	PTK2	Q05397	CHEMBL2695	Kinase	0.074392272	101 / 15
Tyrosine-protein kinase SRC	SRC	P12931	CHEMBL267	Kinase	0.074392272	172 / 38
Dual specificity protein kinase TTK	TTK	P33981	CHEMBL3983	Kinase	0.074392272	54 / 2
Protein tyrosine kinase 2 beta	PTK2B	Q14289	CHEMBL5469	Kinase	0.074392272	36 / 21
Vascular endothelial growth factor receptor 2	KDR	P35968	CHEMBL279	Kinase	0.074392272	753 / 124
MAP kinase ERK2	MAPK1	P28482	CHEMBL4040	Kinase	0.074392272	388 / 5

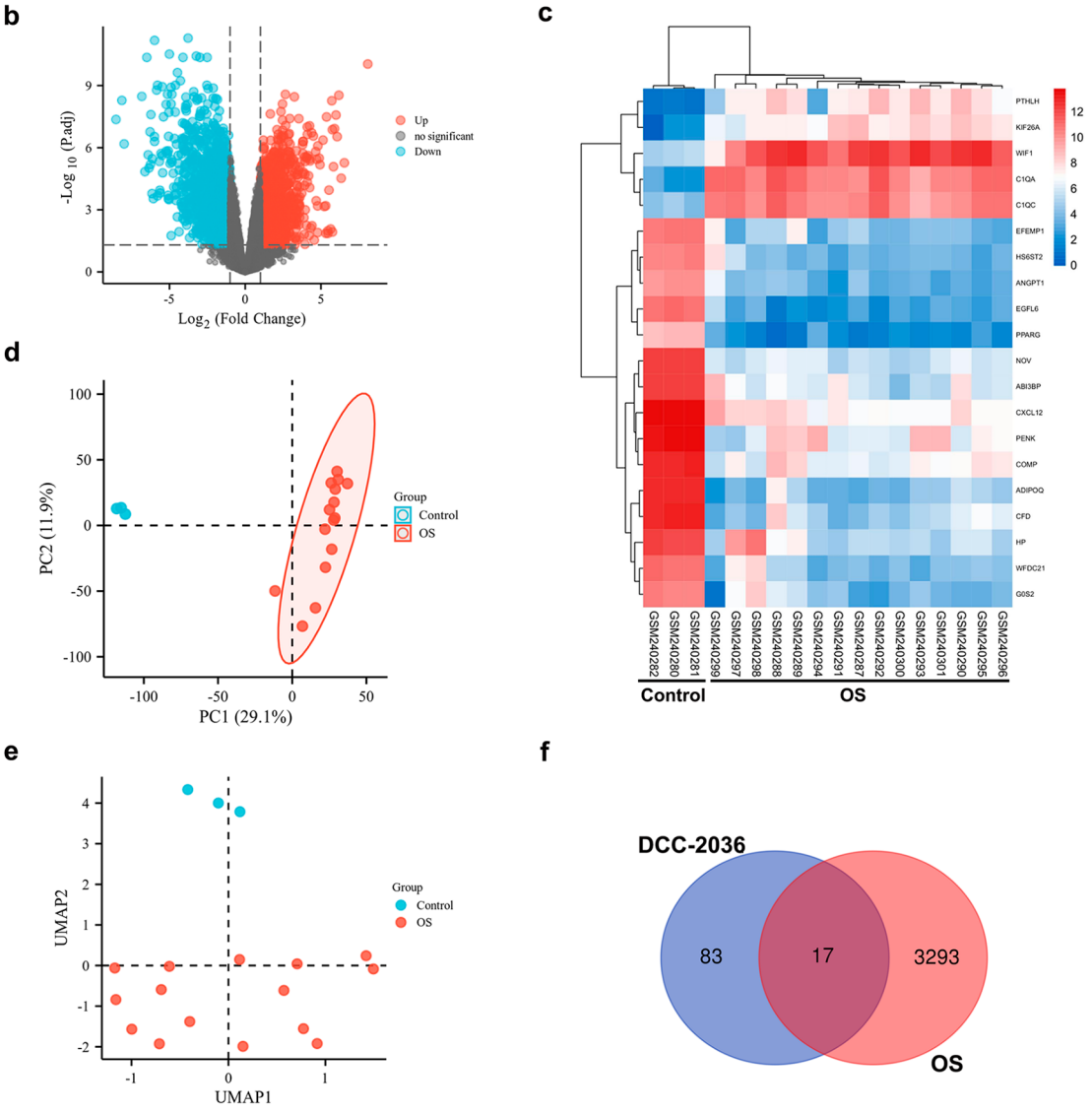

Fig. 3 (See legend on next page.)

(See figure on previous page.)

Fig. 3 Network pharmacology evaluation of the potential targets of DCC-2036 for application in osteosarcoma **a**. The DCC-2036 SMILES notation was obtained from PubChem: (CC(C)(C)C1 = NN(C(= C1)NC(= O)NC2 = C(C = C(C = C2)OC3 = CC(= NC = C3)C(= O)NC)F)C4 = CC5 = C(C = C4)N = CC = C5). Using this SMILES notation, the potential targets of DCC-2036 were predicted on the SwissTargetPrediction website (https://swissmodel.expasy.org/). **(b)** Volcano plot analysis of gene expression differences is presented; red dots indicate genes with high expression, gray dots represent genes with no significant change, and blue dots indicate genes with low expression. Significance was determined at $p < 0.05$, with log2(Fold Change) OS vs. OB ≥ 1. **(c)** The heat map indicates gene expression levels, with red representing high expression and blue representing low expression. **d-e.** PCA (Principal Component Analysis) and UMAP (Uniform Manifold Approximation and Projection) diagrams illustrate the distribution of samples. A greater distance between samples in different groups indicates a larger difference between those groups. **(d)** PCA diagram and **(e)** UMAP diagram. **f.** Venn diagram illustrating the intersection between the 100 effective targets of DCC-2036 and 3,310 differentially expressed genes

significant differential expression. The criteria for gene selection were established as|log2Fold Change| ≥ 1 and FDR < 0.05 (Fig. 5a). Furthermore, KEGG analysis indicated that autophagy was the most enriched pathway influenced by DCC-2036 treatment, with a strong association to lysosomal function (Fig. 5b). To validate the role of DCC-2036 in regulating autophagy, we conducted an immunofluorescence assay. The results of the immunofluorescence staining demonstrated a transition of LC3B fluorescence from a diffuse state to a speckled state, indicative of autophagy activation by DCC-2036 (Fig. 5c). Additionally, western blot analysis confirmed that DCC-2036 significantly reduced p62 protein expression while increasing LC3B-II levels in 143B cells, further supporting the enhancement of autophagy (Fig. 5d). As shown in Fig. 5d, the ratio of LC3B II to LC3B I increased in a concentration-dependent manner.

To further investigate whether the activation of autophagy mediates the inhibitory effects of DCC-2036 on osteosarcoma cells, we treated 143B cells with DCC-2036 while co-administering the autophagy inhibitor 3-MA. Our findings demonstrated that, in comparison to the DCC-2036 treatment group, the cell growth activity, clonogenicity, migration, and invasion capabilities were significantly enhanced in the 3-MA combination group (Fig. 6a-c), while apoptosis was suppressed (Fig. 6d). Moreover, Western blot analysis confirmed that the inclusion of the autophagy inhibitor 3-MA in the treatment of 143B cells markedly increased the expression of P62 protein and decreased the expression of LC3B-II (Fig. 6e). Collectively, these results indicate that DCC-2036 effectively inhibits the activity of osteosarcoma cells by inducing autophagy.

The PI3K-AKT-mTORC1 signaling pathway plays a critical role as both an upstream signal in the inhibition of autophagy and a downstream regulatory pathway of HCK [21–24]. Western blot analysis revealed a significant reduction in the phosphorylation of AKT (p-AKT), S6K (p-S6K), and 4EBP1 (p-4EBP1), which are key signaling molecules within the PI3K-AKT-mTORC1 pathway, following treatment with various concentrations of DCC-2036. Notably, the inhibitory effects became more pronounced with increasing drug concentration (Fig. 7a). Furthermore, subsequent Western blot analysis indicated that the addition of the mTOR activator MHY1485 to 143B cells significantly elevated the protein expression levels of key signaling molecules within the PI3K-AKT-mTORC1 pathway compared to the DCC-2036 treatment group. Additionally, there was a notable increase in the expression of the autophagy-related marker protein p62 and a significant decrease in LC3B-II expression in the MHY1485 combination group (Fig. 7b), suggesting that DCC-2036 activates autophagy in osteosarcoma cells by inhibiting the PI3K-AKT-mTORC1 signaling pathway.

DCC-2036 inhibits the growth of xenografted 143B cells in BALB/C-nude mice

To further investigate the role of DCC-2036 in vivo, 143B cells were subcutaneously transplanted into nude mice. Following tumor dissociation, the tumor volume in the control group was significantly larger than that in the DCC-2036 group (Fig. 8a). Tumor volume and body weight of the mice were measured on the 7th day post-inoculation. Starting on day 7 and continuing until day 28, DCC-2036 or sodium carboxymethylcellulose combined with Tween 80 was administered intragastrically to the mice. The tumor growth curve and body weight change curve indicated that the tumor volume in the DCC-2036 group was significantly lower than that in the control group, while no significant difference in body weight was observed (Fig. 8b). This suggests the efficacy and safety of DCC-2036 in treating osteosarcoma. Furthermore, immunohistochemical analysis of p-HCK, HCK, P62, and LC3B expression in tumor tissues revealed a decrease in p-HCK, HCK, and P62 levels, along with an increase in LC3B levels in response to DCC-2036 (Fig. 8c). Immunoblotting of xenograft tissues from the mice demonstrated that DCC-2036 enhances autophagy through the inactivation of the PI3K-AKT-mTOR pathway, thereby suppressing the growth of 143B tumors, which is consistent with the in vitro data (Fig. 8d).

Discussion

Currently, combined therapies involving surgical intervention and chemotherapy have resulted in a long-term survival rate of 60–70% for osteosarcoma patients. However, patients with local relapse or distal metastasis exhibit resistance to conventional chemotherapy, leading to an overall 5-year survival rate of approximately 20% or

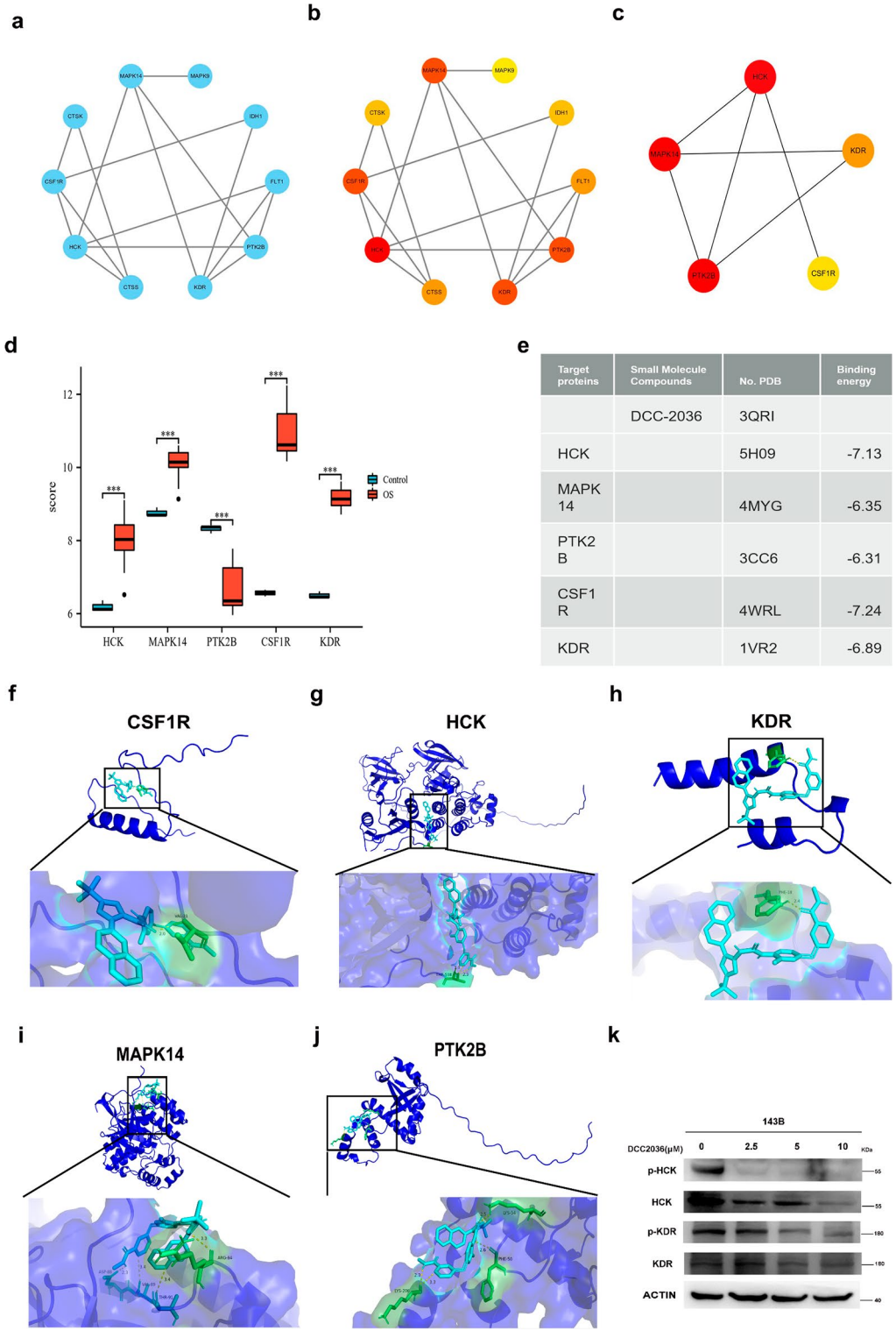

Target proteins	Small Molecule Compounds	No. PDB	Binding energy
	DCC-2036	3QRI	
HCK		5H09	-7.13
MAPK 14		4MYG	-6.35
PTK2 B		3CC6	-6.31
CSF1 R		4WRL	-7.24
KDR		1VR2	-6.89

Fig. 4 Illustrates the construction of a protein-protein interaction network diagram, topological analysis, expression grouping of key differentially expressed genes (DEGs), and visualization of DCC-2036 binding with these key DEGs **a.** The protein interaction network diagram depicts ten potential target genes. **b-c.** Topological analysis shows that the intensity of the red color in the target nodes correlates with their Degree value, indicating a stronger interaction capability with other targets. In contrast, targets exhibiting a more yellow color possess a lower Degree value. **d**. A comparison of the expression levels of HCK, MAPK14, PTK2B, KDR, and CSF1R between the control group and the OS group was performed using mean ± SD and Student's t-test (***, $p < 0.001$). **e.** The binding energy values of HCK, MAPK14, PTK2B, KDR, CSF1R, and DCC-2036 were analyzed. **f-j.** The 2D docking visualization of DCC-2036 with HCK, MAPK14, PTK2B, KDR, and CSF1R is presented. **k.** 143B cells were treated with DCC-2036 at varying concentrations (0 μM, 2.5 μM, 5 μM, 10 μM) for 48 h, and changes in HCK/KDR phosphorylation and total protein levels were assessed using western blot analysis

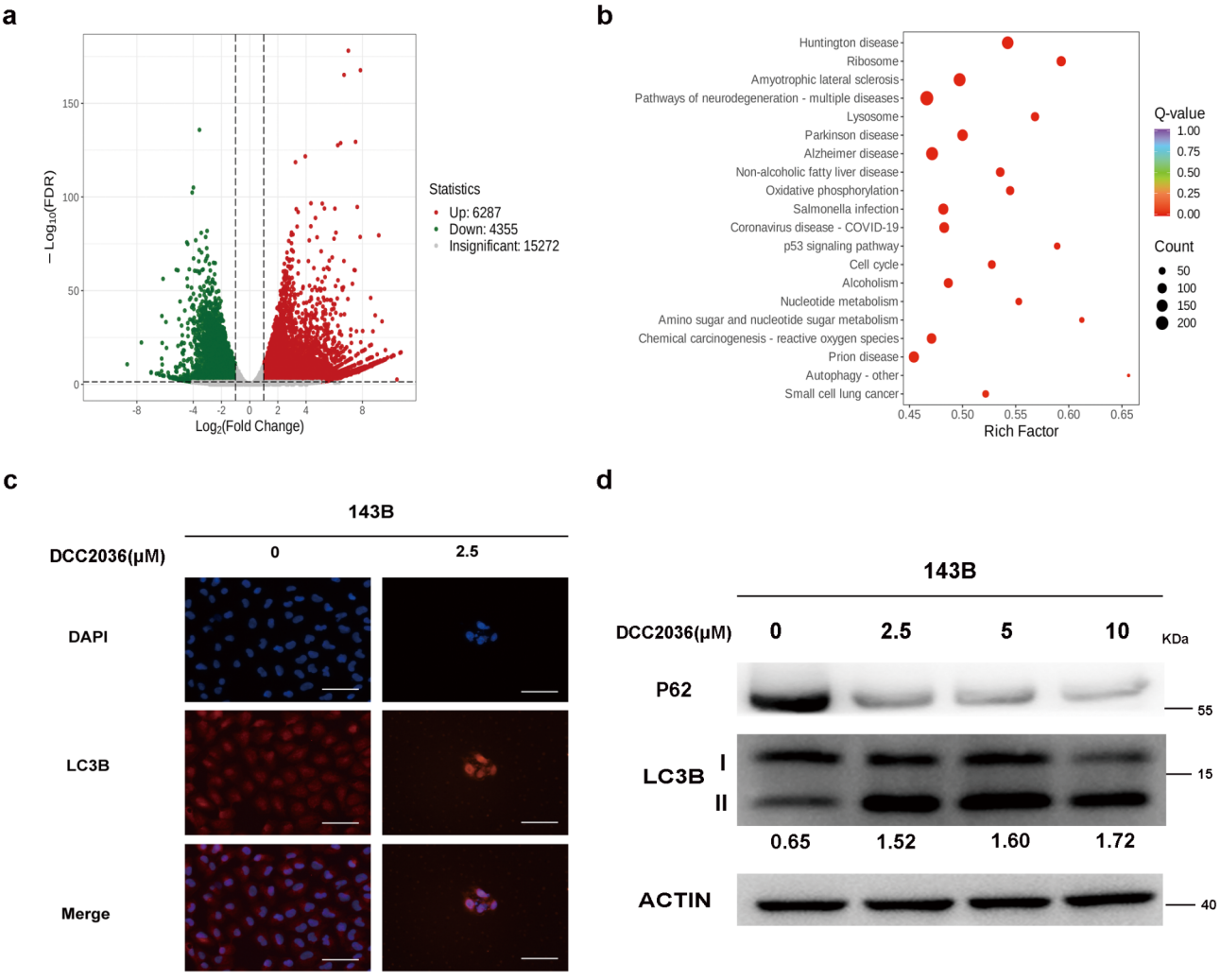

Fig. 5 DCC-2036 activates autophagy in osteosarcoma cells **a.** The volcano plot illustrates differential gene expression, with the horizontal axis depicting the fold change in gene expression and the vertical axis representing the significance level of differentially expressed genes. Up-regulated genes are indicated by red dots, down-regulated genes by green dots, and non-differentially expressed genes by gray dots. **b.** The distribution plot of KEGG enrichment displays KEGG pathways on the vertical axis and the Rich factor, which indicates the degree of enrichment, on the horizontal axis. Larger dots correspond to a greater number of pathway-enriched differential genes, while the color intensity of each dot reflects the significance of enrichment. **c**. An immunofluorescence assay was performed to assess the state of autophagy in 143B cells treated with varying concentrations of DCC-2036 (0 μM and 2.5 μM) for 48 h. A scale bar of 100 μm is included for reference. **d.** A Western blot assay was conducted to evaluate changes in autophagy-related marker proteins in 143B cells treated with different concentrations of DCC-2036 (0 μM, 2.5 μM, 5 μM, and 10 μM) for 48 h. Gray value analyses were employed to quantify the LC3B II / LC3B I ratios

less [25, 26]. Therefore, there is an urgent need to develop new therapeutic strategies for osteosarcoma patients, particularly given their poor prognosis and the disease's prevalence among children and adolescents.

DCC-2036, a novel third-generation tyrosine kinase inhibitor (TKI), possesses a broader kinase inhibition profile compared to second-generation TKIs such as sorafenib [18]. Our previous studies have demonstrated that DCC-2036 has the potential to inhibit triple-negative breast cancer (TNBC) by suppressing AXL, MET, and KLF5 [19, 20]. Additionally, in vitro kinase assays indicated that DCC-2036 effectively inhibits multiple targets, including SRC, PDGFRα, and VEGFR2/KDR, all of which are activated and/or highly expressed in osteosarcoma [18, 27]. This research confirms that DCC-2036 efficiently inhibits osteosarcoma both in vitro and in vivo. First, DCC-2036 exhibited potent antiproliferative activity and reduced the colony-forming capability in osteosarcoma cell lines (143B and MG63). It's worth noting that the IC50 values of DCC-2036 for inhibiting the proliferation of osteosarcoma cell lines 143B and MG63 were 2.59 μM and 1.431 μM, respectively, according to the CCK8 assay (Fig. 1a). However, the IC50 values of paclitaxel (PTX) and cisplatin (DDP) for inhibiting the proliferation of MG63 were 4.11 μM and 5.07 μM [28], and the IC50 value of cisplatin for inhibiting the proliferation of

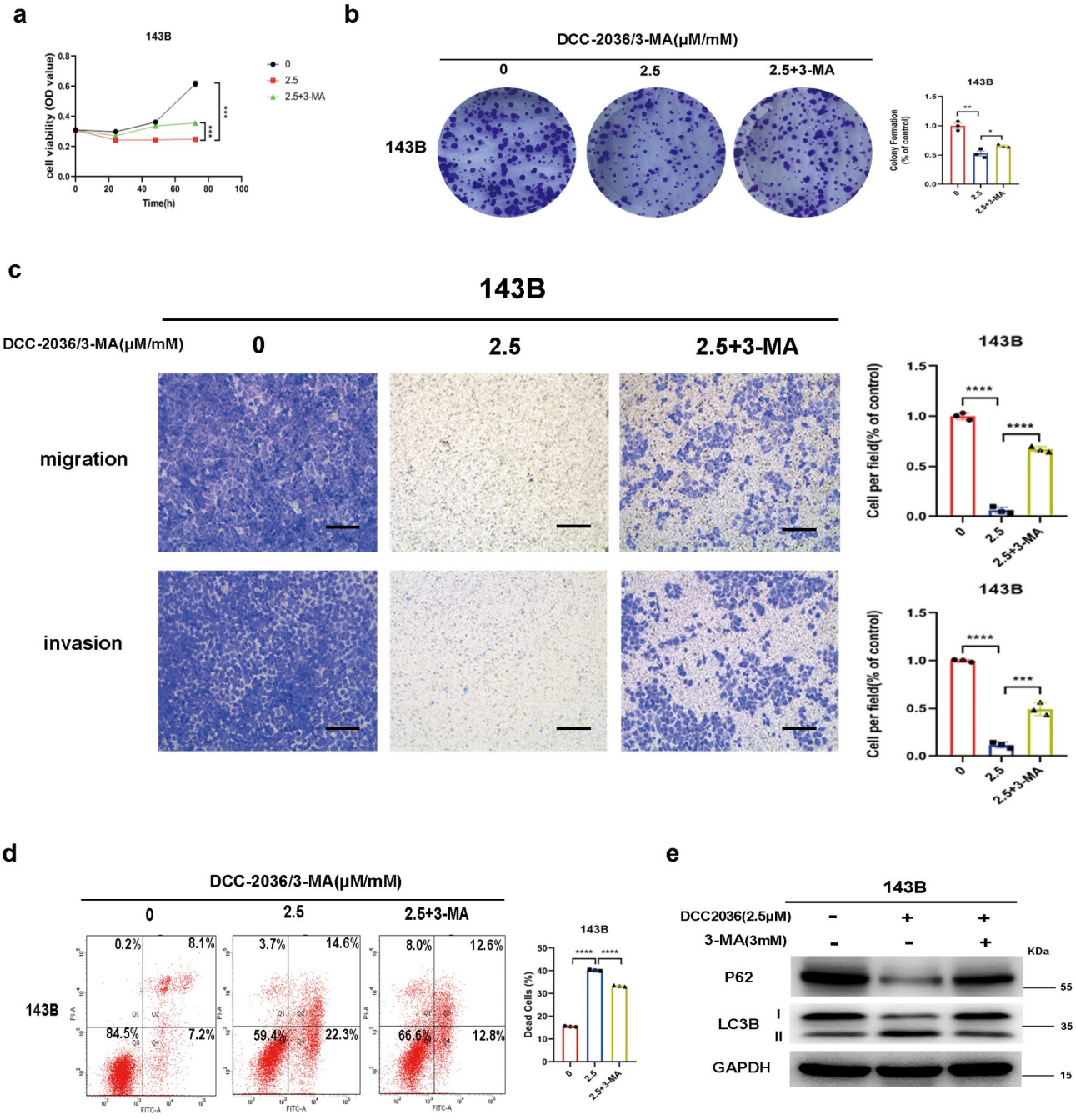

Fig. 6 DCC-2036 inhibits the activity of osteosarcoma cells by activating autophagy **(a)** The control group was treated with 0 μM, the treatment group received DCC-2036 (2.5 μM), and the combined treatment group was administered DCC-2036 (2.5 μM) alongside 3-MA (3 μM). Osteosarcoma cells were exposed to DCC-2036 (2.5 μM) for 48 h, followed by the addition of 3-MA (30 μM) for an additional 3 h. The growth activity of the three cell groups was assessed using the CCK8 assay at 0, 24, 48, and 72 h. (**b**-**e**) Cell treatment and grouping as described in **(a)**. **(b)** Cells were subjected to three independent experiments to quantify the number of cell colonies. The left graph illustrates a representative result from these experiments, while the right graph presents a statistical analysis of the number of clones. **(c)** A Transwell assay was utilized to evaluate the invasion and migration of treated 143B cells. The left diagram shows a representative result from three independent experiments, and the right diagram provides a statistical analysis of cell numbers. Magnification was set at 400× with a scale bar of 100 μm. **(d)** An Annexin V-FITC/PI double dye flow assay was performed to quantify cell death rates. The left graph depicts a representative result from three independent experiments, while the right graph displays a statistical analysis. **(e)** A Western blot assay was conducted to detect changes in markers related to autophagy

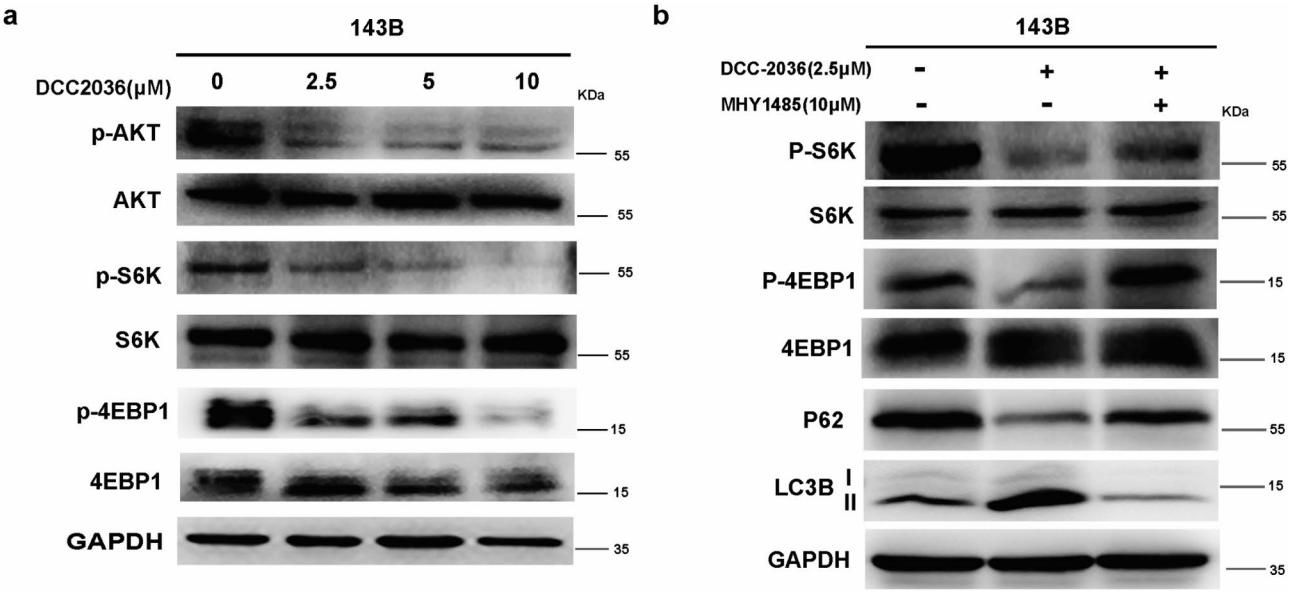

Fig. 7 DCC-2036 activates autophagy in osteosarcoma cells by inhibiting the PI3K-AKT-mTORC1 signaling pathway **(a)** Following treatment of 143B cells with DCC-2036 at varying concentrations (0 μM, 2.5 μM, 5 μM, 10 μM) for 48 h, the phosphorylation levels of AKT, S6K, 4EBP1, and total protein levels were assessed using western blot analysis. **(b)** The control group, treatment group (DCC-2036 at 2.5 μM), and combined treatment group (DCC-2036 at 2.5 μM + MHY1485 at 10 μM) were evaluated. After 48 h of DCC-2036 treatment, osteosarcoma cells were subsequently treated with MHY1485 for 6 h. The protein expression of key signaling molecules within the PI3K-AKT-mTORC1 pathway and the alterations in autophagy-related marker proteins were analyzed through western blot assay

143B were more than 5 μM [29]. Therefore, DCC-2036 was more effective than cisplatin and paclitaxel in osteosarcoma cells. Second, DCC-2036 induced apoptosis and inhibited epithelial-mesenchymal transition (EMT), as well as the migration and invasion of 143B and MG63 cells. Third, DCC-2036 inhibited the growth of xenografted 143B cells in BALB/C nude mice.

To identify the primary target of DCC-2036 in osteosarcoma (OS) cells, we initially performed a network pharmacology study. Effective targets of DCC-2036 were identified using the Swiss database, followed by differential enrichment analysis on osteoblastoma (OB) and osteosarcoma (OS) datasets from the GEO database. A total of 17 potential differentially expressed genes (DEGs) were identified, including HCK, CTSK, TRPV1, FLT1, PDE4B, IDH1, PTK2B, ACACA, MERTK, MAPK9, MAPK14, CTSS, CDC42BPG, TNKS, KDR, PDE11A, and CSF1R, indicating that these genes may serve as potential targets for DCC-2036 in the inhibition of osteosarcoma. Subsequently, an interaction analysis of the 17 potential target genes was conducted using the String database, which revealed interactions among 10 of these genes. Topological analysis was performed using the Cytohubba plugin, identifying the top five genes with the strongest interaction capabilities: HCK, MAPK14, PTK2B, KDR, and CSF1R. Furthermore, molecular docking studies were conducted by integrating multiple databases and utilizing AutodockTools software to dock DCC-2036 with HCK, MAPK14, PTK2B, KDR, and CSF1R. The results indicated that HCK, MAPK14, PTK2B, KDR, and CSF1R successfully completed docking with DCC-2036 under physiological conditions. The findings indicated five potential key targets of DCC-2036 in osteosarcoma: HCK, MAPK14, PTK2B, CSF1R, and KDR. Based on the in vitro kinase assay for DCC-2036, only the IC50 values for HCK (40 nM) and KDR (4 nM) were below 100 nM [18]. Subsequently, we observed a significant decrease in the ratio of p-HCK to HCK, while the ratio of p-KDR to KDR exhibited only minor changes following DCC-2036 treatment, as determined by Western blot (WB) assay. HCK, a member of the SRC family, has been reported to play a crucial role in the proliferation, apoptosis, invasion, and metastasis of osteosarcoma [30]. Therefore, we propose that HCK may serve as the critical target of DCC-2036 in osteosarcoma.

To investigate the specific mechanism of DCC-2036 in osteosarcoma (OS) cells, RNA sequencing was performed, revealing that autophagy was the most enriched pathway (Rich factor) following DCC-2036 treatment, and it was closely associated with lysosomal activity. Subsequently, Western blot (WB) assays of P62 and LC3B, along with LC3 spot assays, indicated that DCC-2036 activated autophagy in osteosarcoma cells. However, autophagy is a double-edged sword in cancer, including osteosarcoma [31, 32]. On one hand, osteosarcoma cells exploit autophagy to promote proliferation, develop resistance to therapy, and protect cancer stem cells. Conversely, autophagy can inhibit the proliferation

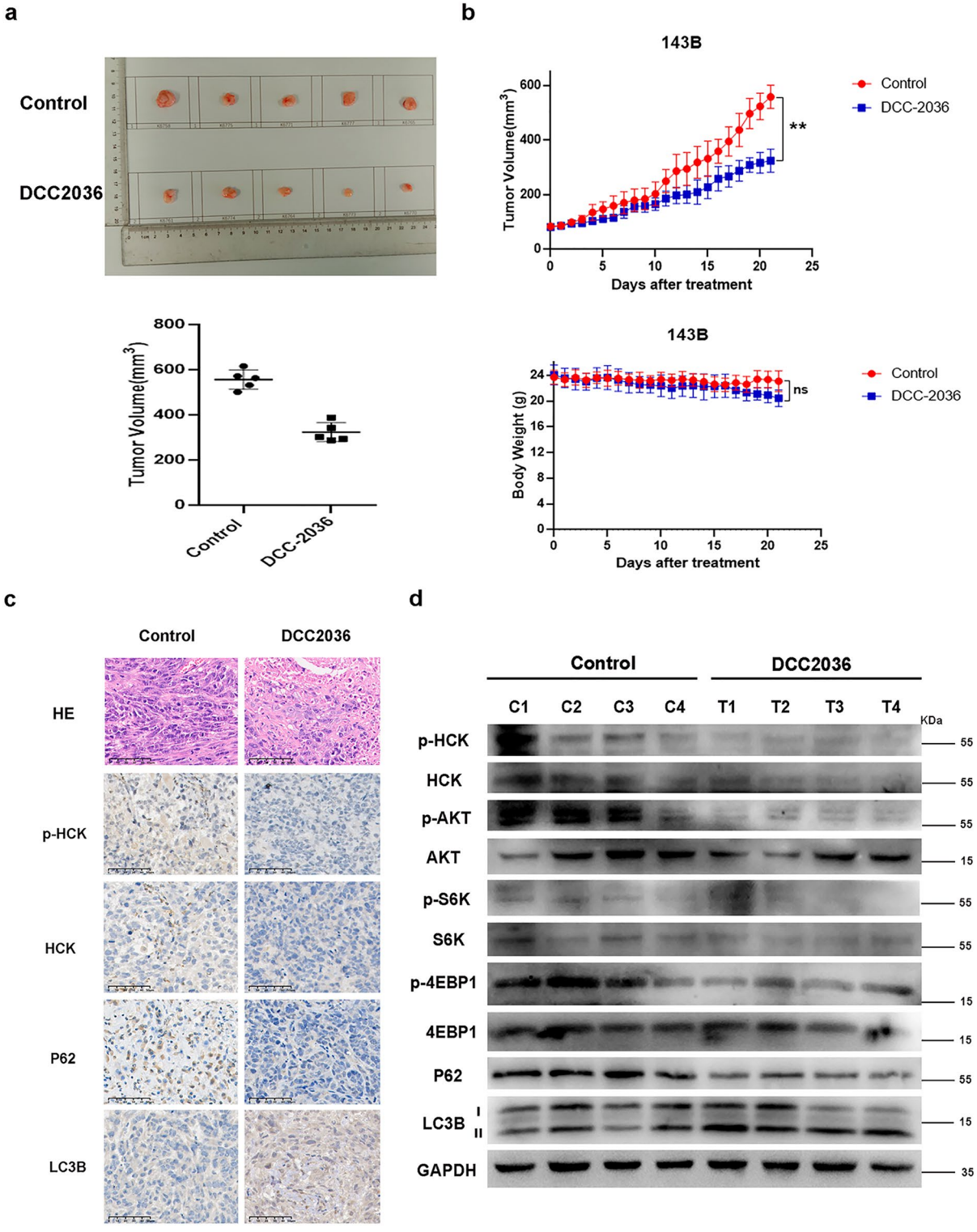

Fig. 8 DCC-2036 inhibits the growth of xenografted 143B cells in BALB/C-nude mice **a**, Representative images of subcutaneous tumor size in mice at the conclusion of the experiment (upper panel) alongside a statistical chart of tumor volume (lower panel). **b**, Subcutaneous tumor growth curve of 143B cells in BALB/C-nude mice, where 2×10^6 cells mixed with Matrigel were xenografted subcutaneously into BALB/C-nude mice. The tumor volume (in mm^3) was measured one week later (upper panel). Additionally, body weight curves of BALB/C-nude mice throughout the experiment are presented (lower panel). **c**, Representative images of hematoxylin and eosin (HE) staining, as well as immunohistochemical staining for p-HCK, HCK, P62, and LC3B expression. **d**, Immunoblotting was conducted on xenografted tumor tissues following the experiment, with tumor tissues selected randomly

and metastasis of osteosarcoma by inducing autophagic cell death, apoptosis, and necrosis [33]. For instance, HSP90AA1-mediated autophagy promotes drug resistance in osteosarcoma [34], however, Aurora-B knockdown inhibits osteosarcoma metastasis by inducing autophagy via the mTOR/ULK1 pathway [35], 11-O-Galloyl Bergenin from Corylopsis coreanas leaves induces autophagy and apoptosis in human osteosarcoma [36]. To confirm the relationship between autophagy and DCC-2036's anti-tumor activity in OS cells, we used 3-MA, which is an inhibitor of autophagy. The result showed that 3-MA could reverse DCC-2036's anti-tumor activity (proliferation, migration, invasion, apoptosis) in part, indicating DCC-2036 exerted anti-tumor activity in OS cells mainly through inducing autophagy but not suppressing autophagy. Autophagy in this study is more likely to inhibit osteosarcoma. Recent studies have investigated the correlation and crosstalk between autophagy and EMT. On one hand, autophagy is essential for maintaining cell survival during EMT. On the other hand, autophagy can inhibit EMT, thereby preventing cells from adopting a mesenchymal phenotype [37, 38]. For example, autophagy can degrade the SNAI1 protein, an EMT-related nuclear transcription factors, so inhibiting autophagy induces EMT [39]. In this study, we have found DCC-2036 could inhibit EMT of 143B and MG63 cells, and DCC-2036 could activate autophagy. Based on the above literature, it is reasonable to speculate that DCC-2036 may inhibit EMT by activating autophagy, but further experiments are needed to confirm this.

Considering that the PI3K/AKT/mTORC1 pathway is not only a classical signaling pathway that suppresses autophagy [23, 24] but also a downstream signaling pathway of HCK [21, 22], we examined the expression of key proteins in the PI3K/AKT/mTORC1 pathway using WB. DCC-2036 was found to inhibit the expression of p-Akt, p-S6K, and p-4EBP1; moreover, the mTOR agonist MHY1485 was able to rescue the autophagy induced by DCC-2036. Therefore, it can be concluded that DCC-2036 induces autophagy in OS cells primarily through the AKT/mTORC1 pathway.

Conclusions

In summary, these data demonstrate that DCC-2036 exhibits potent activity against osteosarcoma (OS) cells by targeting the HCK/AKT/mTORC1 axis to induce autophagy both in vivo and in vitro, without any significant toxicity. Therefore, DCC-2036 is a promising candidate for targeting OS characterized by HCK overexpression.

Supplementary Information

The online version contains supplementary material available at https://doi.org/10.1186/s12957-025-03778-2.

Supplementary Material 1

Supplementary Material 2

Supplementary Material 3

Supplementary Material 4

Author contributions

J.H. Writing original draft. J.H. and L.Y.Y. Designed and performed most of the experiments. Q.Y. Analyzed data. X.T.S. provided ideas and critical comments. Y.Y.S. Writing– review & editing. Z.L.D. conceived and directed the project.

Funding

This work was supported by the Project of National Natural Science Foundation of China (81972487), Project of Natural Science Foundation of Hunan Province (2024JJ9408, 2022JJ70038), Project of Health Commission of Hunan Province (202104070680).

Data availability

Sequence data that support the findings of this study have been deposited in the NCBI SRA database with the primary accession code PRJNA1142215.

Declarations

Ethical approval

The Medical Ethics Committee of the Nanhua Hospital, University of South China approved all animal experiments (2023-KY-120).

Competing interests

The authors declare no competing interests.

Author details

[1]Department of Orthopaedic Surgery, Second Affiliated Hospital of Chongqing Medical University, Chongqing 400072, PR China
[2]The Nanhua Affiliated Hospital, Department of Spine Surgery, Hengyang Medical School, University of South China, Hengyang, Hunan 421001, China
[3]The First Affiliated Hospital, Cancer Research Institute, Hengyang Medical School, University of South China, Hengyang, Hunan 421001, P.R. China

Received: 9 January 2025 / Accepted: 25 March 2025
Published online: 02 April 2025

References

1. Li L, Li Z, He X, Wang Y, Lu M, Gong T, et al. A nutritional metabolism related prognostic scoring system for patients with newly diagnosed osteosarcoma. Front Nutr. 2022;9:883308.
2. Liu Y, Qiu G, Luo Y, Li S, Xu Y, Zhang Y, et al. Circular RNA ROCK1, a novel circrna, suppresses osteosarcoma proliferation and migration via altering the miR-532-5p/PTEN axis. Exp Mol Med. 2022;54(7):1024–37.
3. Ma W, Xue N, Zhang J, Wang D, Yao X, Lin L, et al. circUBAP2 regulates osteosarcoma progression via the miR–204–3p/HMGA2 axis. Int J Oncol. 2021;58(3):298–311.
4. Li J, Su L, Xiao X, Wu F, Du G, Guo X, et al. Development and validation of novel prognostic models for Immune-Related genes in osteosarcoma. Front Mol Biosci. 2022;9:828886.
5. Gong G, Ganesan K, Xiong Q, Zheng Y. Anti-Invasive and Anti-Migratory effects of Ononin on human osteosarcoma cells by limiting the MMP2/9 and EGFR-Erk1/2 pathway. Cancers. 2023;15(3):758.
6. Pan Z, Li SJ, Guo H, Li ZH, Fei X, Chang SM, et al. Ebastine exerts antitumor activity and induces autophagy by activating AMPK/ULK1 signaling in an IPMK-dependent manner in osteosarcoma. Int J Biol Sci. 2023;19(2):537–51.
7. Wei H, Chen F, Chen J, Lin H, Wang S, Wang Y, et al. Mesenchymal stem cell derived exosomes as nanodrug carrier of doxorubicin for targeted osteosarcoma therapy via SDF1-CXCR4 axis. Int J Nanomed. 2022;17:3483–95.
8. Sirikul W, Buawangpong N, Pruksakorn D, Charoentum C, Teeyakasem P, Koonrungsesomboon N. The survival outcomes, prognostic factors and

adverse events following systemic chemotherapy treatment in bone sarcomas: A retrospective observational study from the experience of the cancer referral center in Northern Thailand. Cancers. 2023;15(7):1979.
9. Sui M, Xiong M, Li Y, Zhou Q, Shen X, Jia D, et al. Cancer therapy with Nanoparticle-Medicated intracellular expression of peptide CRM1-Inhibitor. Int J Nanomed. 2021;16:2833–47.
10. Hong C, Wei J, Zhou T, Wang X, Cai J. FGFR2-ERC1: A subtype of FGFR2 oncogenic fusion variant in lung adenocarcinoma and the response to anlotinib. OncoTargets Therapy. 2022;15:651–7.
11. Sun H, Tonks NK. The coordinated action of protein tyrosine phosphatases and kinases in cell signaling. Trends Biochem Sci. 1994;19(11):480–5.
12. Papadopoulos S, Koulouris P, Royer-Chardon C, Tsoumakidou G, Dolcan A, Cherix S, et al. Case report: tyrosine kinase inhibitors induced lymphadenopathy in desmoid tumor patients. Front Endocrinol. 2022;13:794512.
13. Makeen HA, Mohan S, Al-Kasim MA, Sultan MH, Albarraq AA, Ahmed RA, et al. Preparation, characterization, and Anti-Cancer activity of nanostructured lipid carriers containing Imatinib. Pharmaceutics. 2021;13(7):1086.
14. Rodia R, Pani F, Caocci G, La Nasa G, Simula MP, Mulas O, et al. Thyroid autoimmunity and hypothyroidism are associated with deep molecular response in patients with chronic myeloid leukemia on tyrosine kinase inhibitors. J Endocrinol Investig. 2022;45(2):291–300.
15. Leibetseder A, Preusser M, Berghoff AS. New approaches with precision medicine in adult brain tumors. Cancers. 2022;14(3):712.
16. Nakano K. Challenges of systemic therapy investigations for bone sarcomas. Int J Mol Sci. 2022;23(7):3540.
17. Gaspar N, Campbell-Hewson Q, Gallego Melcon S, Locatelli F, Venkatramani R, Hecker-Nolting S, et al. Phase I/II study of single-agent lenvatinib in children and adolescents with refractory or relapsed solid malignancies and young adults with osteosarcoma (ITCC-050)(☆). ESMO Open. 2021;6(5):100250.
18. Chan WW, Wise SC, Kaufman MD, Ahn YM, Ensinger CL, Haack T, et al. Conformational control Inhibition of the BCR-ABL1 tyrosine kinase, including the gatekeeper T315I mutant, by the switch-control inhibitor DCC-2036. Cancer Cell. 2011;19(4):556–68.
19. Shen Y, Zhang W, Liu J, He J, Cao R, Chen X, et al. Therapeutic activity of DCC-2036, a novel tyrosine kinase inhibitor, against triple-negative breast cancer patient-derived xenografts by targeting AXL/MET. Int J Cancer. 2019;144(3):651–64.
20. Shen Y, Zhu Q, Xiao M, Yin L, Feng W, Feng J, et al. Inhibitory effect of the novel tyrosine kinase inhibitor DCC-2036 on triple-negative breast cancer stem cells through AXL-KLF5 positive feedback loop. Cell Death Dis. 2022;13(8):749.
21. Yang G, Buhrlage SJ, Tan L, Liu X, Chen J, Xu L, et al. HCK is a survival determinant transactivated by mutated MYD88, and a direct target of ibrutinib. Blood. 2016;127(25):3237–52.
22. Roversi FM, Bueno MLP, Pericole FV, Saad STO. Hematopoietic cell kinase (HCK) is a player of the crosstalk between hematopoietic cells and bone marrow niche through CXCL12/CXCR4 axis. Front Cell Dev Biology. 2021;9:634044.
23. Xu P, Zhang X, Cao J, Yang J, Chen Z, Wang W, et al. The novel role of circular RNA ST3GAL6 on blocking gastric cancer malignant behaviours through autophagy regulated by the FOXP2/MET/mTOR axis. Clin Translational Med. 2022;12(1):e707.
24. Li HL, Deng NH, He XS, Li YH. Small biomarkers with massive impacts: PI3K/AKT/mTOR signalling and MicroRNA crosstalk regulate nasopharyngeal carcinoma. Biomark Res. 2022;10(1):52.
25. Wu W, Zhang Z, Jing D, Huang X, Ren D, Shao Z, et al. SGLT2 inhibitor activates the STING/IRF3/IFN-β pathway and induces immune infiltration in osteosarcoma. Cell Death Dis. 2022;13(6):523.
26. Jiang Y, Wang G, Mu H, Ma X, Wang Z, Lv Y, et al. Bromodomain Inhibition attenuates the progression and sensitizes the chemosensitivity of osteosarcoma by repressing GP130/STAT3 signaling. Front Oncol. 2021;11:642134.
27. Fathizadeh H, Mirzaei H, Asemi Z. Melatonin: an anti-tumor agent for osteosarcoma. Cancer Cell Int. 2019;19:319.
28. Shen P, Cheng Y. Correction: long noncoding RNA LncARSR confers resistance to adriamycin and promotes osteosarcoma progression. Cell Death Dis. 2021;12(5):455.
29. Huang X, Wang W, Li Y. Niclosamide is a potential candidate for the treatment of chemo-resistant osteosarcoma. Genet Mol Biology. 2023;46(1):e20220136.
30. Liu W, Li T, Hu W, Ji Q, Hu F, Wang Q, et al. Hematopoietic cell kinase enhances osteosarcoma development via the MEK/ERK pathway. J Cell Mol Med. 2021;25(18):8789–95.
31. Chen Y, Liang Y, Luo X, Hu Q. Oxidative resistance of leukemic stem cells and oxidative damage to hematopoietic stem cells under pro-oxidative therapy. Cell Death Dis. 2020;11(4):291.
32. Liu B, Yao X, Zhang C, Liu Y, Wei L, Huang Q, et al. PTK6 inhibits autophagy to promote uveal melanoma tumorigenesis by binding to SOCS3 and regulating mTOR phosphorylation. Cell Death Dis. 2023;14(1):55.
33. Ning B, Liu Y, Huang T, Wei Y. Autophagy and its role in osteosarcoma. Cancer Med. 2023;12(5):5676–87.
34. Xiao X, Wang W, Li Y, Yang D, Li X, Shen C, et al. HSP90AA1-mediated autophagy promotes drug resistance in osteosarcoma. J Experimental Clin cancer Research: CR. 2018;37(1):201.
35. Wu X, Liu JM, Song HH, Yang QK, Ying H, Tong WL, et al. Aurora-B knockdown inhibits osteosarcoma metastasis by inducing autophagy via the mTOR/ULK1 pathway. Cancer Cell Int. 2020;20(1):575.
36. Park KR, Kwon YJ, Cho M, Kwon IK, Hong JT, Yun HM. 11-O-Galloyl Bergenin from Corylopsis Coreanas leaves induces autophagy and apoptosis in human osteosarcoma. Am J Chin Med. 2021;49(8):2017–31.
37. Ma J, Ye W, Yang Y, Wu T, Wang Y, Li J, et al. The interaction between autophagy and the epithelial-mesenchymal transition mediated by NICD/ULK1 is involved in the formation of diabetic cataracts. Mol Med (Cambridge Mass). 2022;28(1):116.
38. Ren T, Zheng B, Huang Y, Wang S, Bao X, Liu K, et al. Osteosarcoma cell intrinsic PD-L2 signals promote invasion and metastasis via the RhoA-ROCK-LIMK2 and autophagy pathways. Cell Death Dis. 2019;10(4):261.
39. Hwang JS, Lai TH, Ahmed M, Pham TM, Elashkar O, Bahar E et al. Regulation of TGF-β1-Induced EMT by Autophagy-Dependent energy metabolism in cancer cells. Cancers. 2022;14(19).

Publisher's note